Development and testing of a micro wind tunnel for on-site wind erosion simulations.

Craig L. Strong[1]*, John F. Leys[2], Mike R. Raupach[3], Joanna E. Bullard[4], Hélène A. Aubault[4], Harry J. Butler[5] and Grant H. McTainsh[6]

[1*] Fenner School of Environment & Society, The Australian National University, Canberra ACT 2601 Australia

[2] New South Wales Office of Environment and Heritage, Gunnedah, NSW 2380 Australia

[3] The Climate Change Institute, The Australian National University, Canberra ACT 2601 Australia (deceased)

[4] Department of Geography, Loughborough University, Leicestershire LE11 3TU United Kingdom

[5] School of Agricultural, Computational & Environmental Sciences, University of Southern Queensland, Toowwomba, QLD 4350 Australia

[6] Griffith School of Environment, Griffith University, Nathan Qld 4111 Australia

* craig.strong@anu.edu.au; Phone +61 2 6125 6683; Fax +61 2 6125 0746

Abstract

Wind erosion processes affect soil surfaces across all land uses worldwide. Understanding the spatial and temporal scales of wind erosion is a challenging undertaking because these processes are diverse and highly variable. Wind tunnels provide a useful tool as they can be used to simulate erosion at small spatial scales. Portable wind tunnels are particularly valued because erosion can be simulated on undisturbed soil surfaces in the field. There has been a long history of use of large portable wind tunnels, with consensus that these wind erosion simulation tools can meet real world aerodynamic criteria. However, one consequence of striving to meet aerodynamic reality is that the size of the tunnels has increased, making them logistically difficult to work with in the field and resulting in a tendency to homogenise naturally complex soil surfaces. This homogenisation is at odds with an increasing awareness of the importance that small scale processes have in wind erosion. To address these logistical and surface homogenisation issues we present here the development and testing of a micro wind tunnel (MWT) designed to simulate wind erosion processes at high spatial resolution. The MWT is a duct-type design - 0.05 m tall 0.1 m wide and with a 1.0 m working section. The tunnel uses a centrifugal motor to suck air through a flow-conditioning section, over the working section and then through a sediment collection trap. Simulated wind velocities range from 5 to 18 m s^{-1}, with high reproducibility. Wind speeds are laterally uniform and values of u_* at the tunnel bed (calculated by measuring the pressure gradients within the MWT) are comparable with those of larger tunnels in which logarithmic profiles can be developed. Saltation sediment can be added. The tunnel can be deployed by a single person and operated on slopes ranging from 0-10 degrees. Evidence is presented here that the MWT provides new and useful understanding of the erodibility of rangelands, claypans and ore stockpiles.

Keywords. *Erodibility, Field studies, Dust, Methodology, Land use, rangelands, mine storage facilities.*

1 Introduction

Wind erosion is widespread across natural and anthropogenic surfaces and occurs worldwide where wind speeds exceed the threshold velocity required to detach soil or sediment particles and transport them. The susceptibility of a surface to wind erosion can be measured in a variety of ways including field-based monitoring of wind regime and sediment transport [1-2], using laboratory or field-based wind tunnels [3-5], portable wind erosion facilities [6] and modelling [7-9]. Each approach has advantages and limitations [5] and this paper focuses on the use of a field wind tunnel.

Despite the increasing variety of techniques available for studying wind erosion, wind tunnels, which are one of the earliest approaches [10], are still very widely used. The usefulness and validity of wind tunnels depends on them adequately simulating the natural processes of wind and for this reason they have typically been constructed to be as large as possible to minimize scaling effects [11]. Whilst fixed location, stationary wind tunnels used for aeolian research can be very large, for example the Chinese Academy of Sciences has a 38 m lab based tunnel [12], their limitation is that they are generally only used with artificial soil surfaces. In contrast, portable wind tunnels typically have an open floor, and can be moved around in the field to simulate wind erosion of surfaces *in situ*. Van Pelt et al. [5] provide a useful review of portable wind tunnels used in wind erosion research and highlight that although these tunnels are ‘portable’ they are often large (e.g. cross-section up to 1 m^2 and length over 10 m) and require considerable logistical support for deployment. Large portable tunnels also have the disadvantage of requiring space around the tunnel for locating generators, trucks, trailers and ancillary equipment.

In many situations it is difficult and expensive to deploy such large wind tunnels in the field due to physical limitations of; site access (e.g. unmade roads), steepness of slopes (e.g. on mine spoils), and cost of labour required to rig and operate the tunnel. Also, on vegetated field sites aerodynamic ‘noise’ is introduced because of difficulties in achieving a good seal between the soil surface and the tunnel [13]. The working section beneath large tunnels can also homogenise the effects of spatial variations in soil surfaces, such as changes in sediment size and soil crust characteristics [14]. Some small portable wind tunnels have been developed and successfully used in the field. For example the wind tunnel constructed by Gillette [15] had a small cross section of 150 mm x 150 mm and length of 3 m and was used to determine threshold friction velocities on biological crusted soil surfaces [16-17]. An alternative approach is the Portable In Situ Wind ERosion Lab (PI-SWERL). The PI-SWERL differs from duct-type wind tunnels in that it uses rotating airflow within a 0.57 m diameter cylinder to generate shear stresses on the surface. Despite this fundamental difference, the results from the PI-SWERL compare well with those from conventional duct-type wind tunnels [18].

The present paper describes the development and testing of a new micro wind tunnel (MWT) designed for field simulation of wind erosion on small plots. The MWT is a duct-type design and is novel because it can be deployed by a single person on slopes ranging from 0-10 degrees. Three examples are provided to illustrate the application of the device measuring the erodibility of rangeland and claypan soils, and of stockpiles at an iron ore storage facility.

2 Materials and Methods

Numerous researchers have proposed practical and aerodynamic criteria to be met by the design of portable wind tunnels [19, 20]. These design criteria are summarised by Maurer et al. [13] as

- the tunnel must achieve wind speeds that reflect natural conditions;
- the tunnel should produce realistic aerodynamic flows within;
- the tunnel must be easy to transport, assemble and handle

and the criteria have been recently reviewed by Van Pelt et al. [5]. In addition, for wind erosion studies it is important that the full range of aeolian sediment transport processes (creep, saltation, suspension) can occur, and that saltating grains can be introduced at the upwind end of the working section to simulate the saltation impact process [20].

2.1 Design and Construction

The MWT has seven key components: a motor and tunnel wind velocity regulator, transition, working and exhaust sections, sediment trap, saltation injection tube and wind speed sensors (Figure 1). The motor is a 0.55 kW electric 240-volt induction motor that turns a 280 mm axial fan. The motor creates suction through the tunnel generating a velocity range of 5-18 m s^{-1}. Wind velocity is controlled via a calibrated baffle plate on the motor exhaust; complete blockage of the exhaust produces zero velocity whilst no blockage allows maximum velocity. Air is drawn into the tunnel through an opening 220 x 50 mm which contracts over 250 mm to a cross section 100 x 50 mm thus accelerating and stabilising the airflow. This stabilisation and organisation of airflow continues through the 1100 mm long transition section (aluminium box tube) downwind of which is a 1000 mm long working section. Within the working section the aluminium floor has been removed allowing direct contact between the wind and the soil surface. The top of the working section has a Perspex viewing window. Keyholes drilled in the top at distances of 100, 450 and 900 mm from the upwind end of the working section allow access for velocity measurement instruments (1 mm Dwyer pitot-static tubes) and are sealed with silicone plugs when not in use. Downwind of the working section is the 705 mm long exhaust section in which tunnel wind velocity is measured, wind transported sediment is sub-sampled via the sediment trap and the cross-section changes from rectangular to circular to allow connection to the induction motor. A manually operated flow bypass valve within the exhaust section enables the operator to control when air is drawn through the tunnel. This avoids the ramp up / ramp down wind speeds associated with the motor being turned on/off being drawn across the tested surface. When the flow bypass value is lowered, air is sucked from the roof within the exhaust section, avoiding flow over the working section. Once the motor has reached maximum revolution, the flow bypass valve can be raised redirecting suction (flow) to the tunnel inlet, ensuring desired wind speed is passed over the working section. The total tunnel footprint including all sections is 3050 mm x 120 mm. The generator and tunnel motor are connected via 5 m lengths of ducting (76 mm diameter) and can be positioned away from the operating tunnel. All equipment is contained in four boxes and transported (including the generator) in a standard box trailer (1800 x 1200 mm).

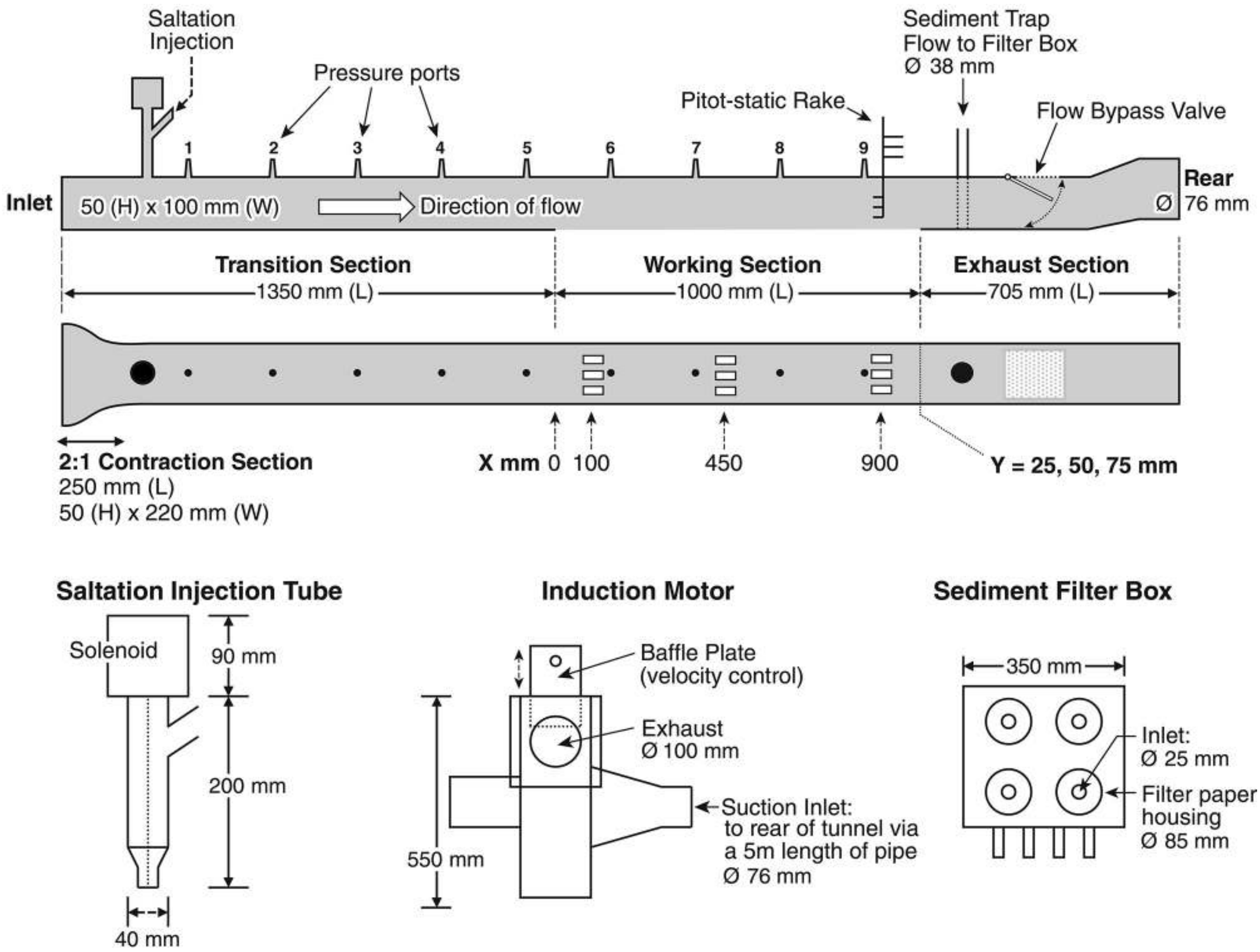

Fig. 1 Schematic diagram of the Micro Wind Tunnel (MWT) displaying the three sections (transition, working and exhaust) and velocity measurement options (pressure ports and pitot-static rake) present. The flow bypass valve enables air to be drawn through the tunnel from the suction induction motor attached at the rear. Sediment transported in the tunnel is subsampled at the sediment trap and collected on filter papers housed in the sediment filter box.

Due to the importance of saltation-impact entrainment in wind erosion of soils [20] saltation material can be added to the wind flow using a saltation injection tube. The injection tube is a 40 mm diameter acrylic tube, positioned at the upwind end of the transition section, which narrows to 2 mm diameter at the base. The injection tube can be opened or sealed using a tapered stainless-steel rod controlled using a solenoid that lifts the rod 10 mm vertically. The solenoid can be activated at the same time as the bypass valve in order to synchronise saltation injection with the start of tunnel flow. Transported sediment is collected via a vertical slot sampler 10 mm wide and 50 mm high. This is located on the centre line of the tunnel and is used to sub sample (10 %) of the sediment-laden tunnel airflow. Air from the sediment sampler is drawn vertically through a 38 mm hose to the sediment filter box which houses 125 mm-diameter glass-fibre filter papers with 0.1 μm pores.

For any one run, wind speed within the tunnel can be measured simultaneously at three different locations using pressure transducers connected to pitot-static tubes or roof mounted pressure ports or a combination of the two. The 1 mm dynamic port Dwyer pitot-static tubes can be positioned in a streamwise array at 100 mm, 450 mm and 900 mm from the upwind end of the working section along the centre line. Alternatively, at each of these locations, they can be arranged crosswise on the centre line and 25 mm from each wall (i.e. 3 equidistance measurements cross-flow). A pitot-static tube can also be located within the sediment trap at the downwind end of the tunnel. The pressure ports are fitted inside the tunnel, flush with the roofline, and located along the centre line at 300 mm intervals in the transition section and 200 mm intervals in the working section (nine in total). The most common field sampling configuration is one pressure transducer connected to a pitot tube at 900 mm upwind at the cross sectional mid-point, one pressure transducer connected to a pitot tube in the sediment sampler and the last pressure transducer connected to opposite end roofline pressure ports (i.e. pressure port numbers one and nine). Where more than three velocity measurements are required to characterise three dimensional flow structures, the tunnel can be run multiple times at a fixed reference velocity with the pressure transducers in different configurations. Data can be made dimensionless by relating all measurements to a fixed reference point. Temperature of the tunnel airflow and barometric air pressure are measured every second and averaged over 1 minute to enable the calculation of air density.

2.2 Airflow Measurements

A range of tests were undertaken to characterise: a) the range of tunnel wind velocities achieved within the tunnel, b) the uniformity of airflow and c) to develop an alternative technique of calculating u_* other than from logarithmic velocity profiles.

Tunnel wind velocity is controlled by raising or lowering the baffle plate on the induction motor exhaust (Figure 1). To determine the relationship between baffle position and tunnel velocity the MWT was run as it would be in the field (i.e. with filters in place) but over a smooth control surface (4 mm ABS plastic sheet, 'glassy' side up). Each baffle position was replicated 19 times and the MWT was run for one minute per replicate. Wind speed was measured using the pitot-static tubes and roof mounted pressure ports. Each baffle position created a different wind speed ranging from 5-18 m s^{-1} with excellent reproducibility (all standard errors lie within +/- 0.002 m s^{-1} of the mean value) (Figure 2).

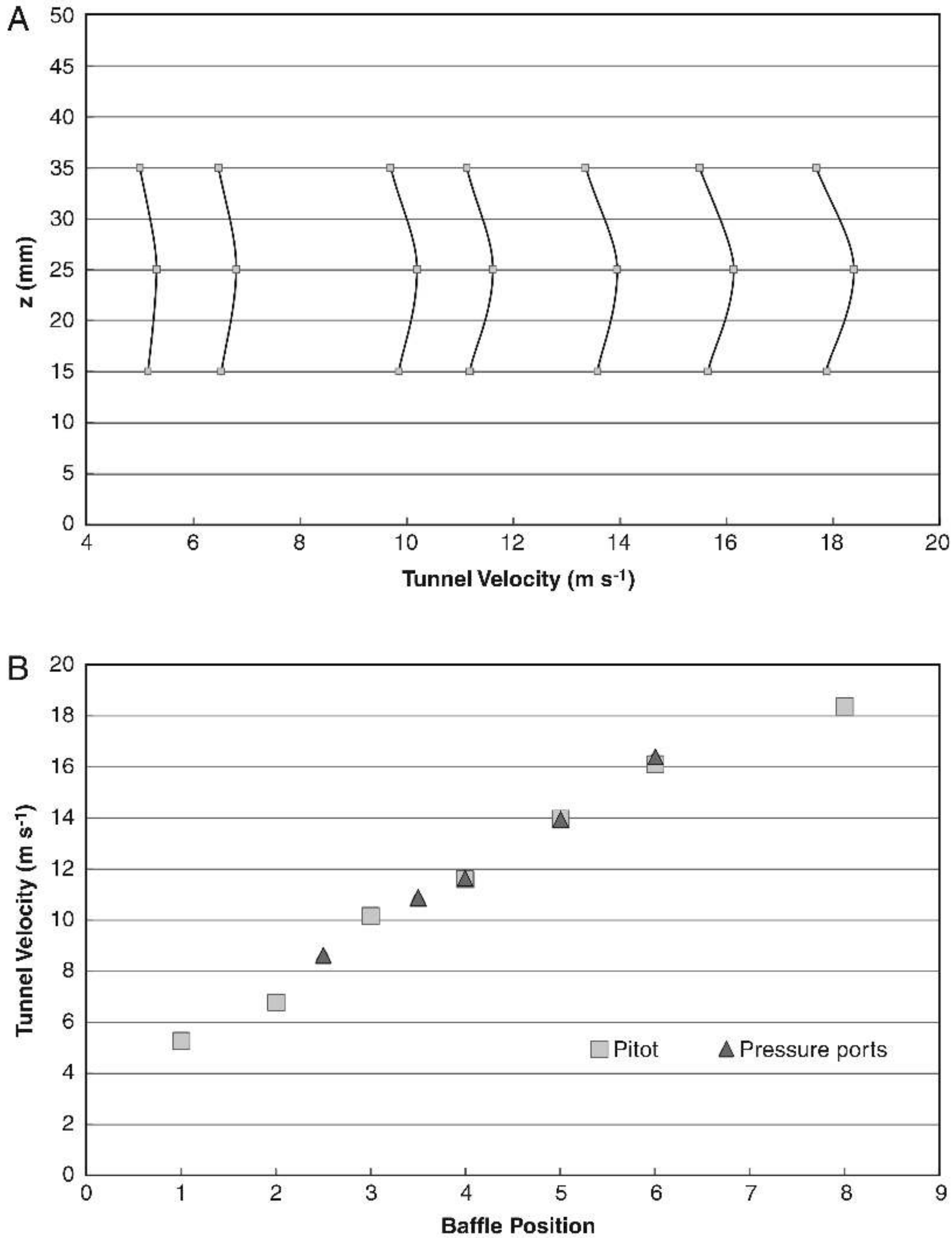

Fig. 2 Airflow velocity (m s^{-1}) is determined by the position of the exhaust baffle. A) Velocity profiles measured with pitot-static tubes over a smooth test surface. Measurements made with a pitot rake at x = 900, y = 50, z = 15, 25 and 35. SE included (19 reps/baffle position). B) Comparison of airflow velocities (m s^{-1}) measured using pitot-static tubes (squares) at x = 900, y = 50, z = 25 (SE included) and pressure port measurements at x = 200 and 900, y = 50, z = 50 (SE included). All testing conducted on the same smooth surface. All standard errors lie within +/- 0.002 m s^{-1} of the mean values

Ideally a wind tunnel should produce uniform airflow across the tunnel and develop a logarithmic profile of wind velocity with height. To test these, with the baffle in position 2.5, wind speed was measured at 25 mm, 50 mm and 75 mm distance across the tunnel (y axis) at 9 different heights (5, 10, 15, 20, 25, 30, 35, 40, 45 mm; z axis) and located at 100 mm, 450 mm and 900 mm from the upwind end of the working section (x axis). This approach provides a grid of 27 velocity measurements at each downwind location and shows how cross-flow uniformity varies with distance down the working section. If all the measurements had been taken simultaneously the instrumentation would have blocked the airflow in the tunnel and set up secondary airflow patterns, so, given the uniformity of wind speeds indicated in Figure 2, measurements were taken at 3 locations at a time for the same baffle position and combined to create the data grid. These tests were repeated over three artificial surfaces, one smooth (ABS plastic as above), one of medium roughness (40 grit sand paper), and one rough (10 mm diameter marbles protruding 2 mm above the test bed).

All surfaces within the tunnel are sources of drag, and the cross-sectional contour plots indicate that changes in floor roughness create the greatest changes in the flow symmetry (Figure 3). As floor roughness increases, flow lines compress near the floor surface. Figure 3 also indicates there is a slight surface imperfection in the top left hand corner where the Perspex working section ceiling is affixed. This has changed the flow symmetry slightly with slower flow along the left side. Despite this, the flow in the tunnel reflects what would be expected in a rectangular duct which is a fully developed flow. The length of the tunnel means this fully developed flow is also turbulent in nature and there is no logarithmic velocity profile as expected in larger wind tunnels.

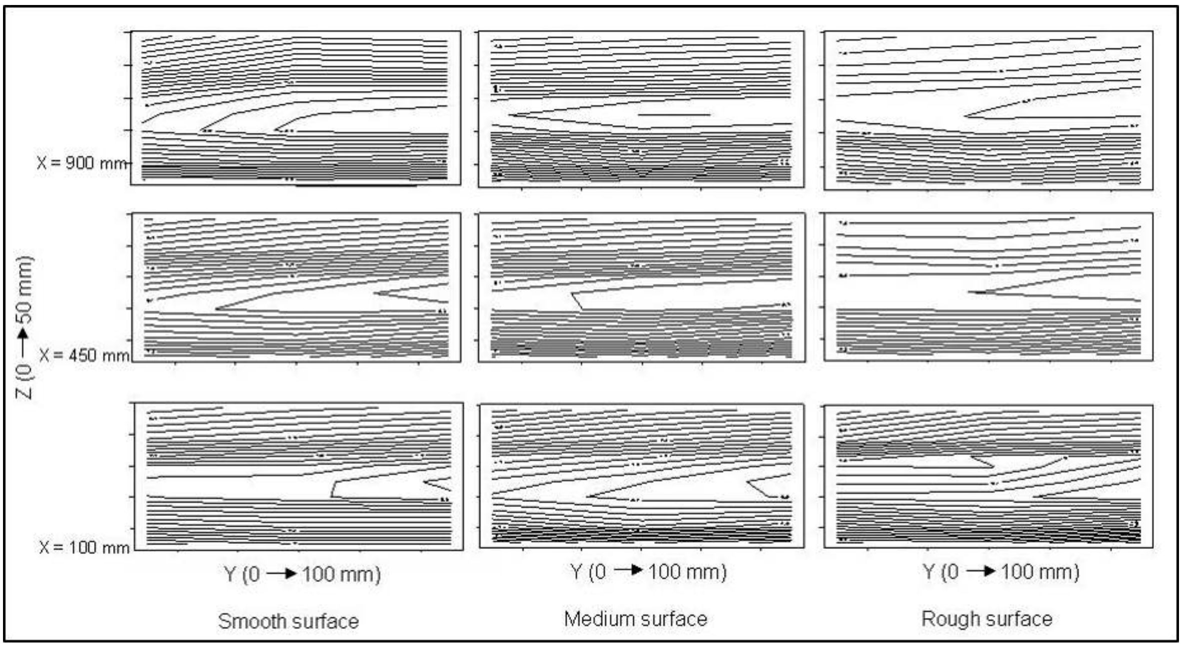

Fig. 3 Contour plots of airflow velocity (0.2 m s^{-1} intervals) for smooth, medium and rough test surfaces showing the cross-sectional profile of the tunnel at 100, 450 and 900 mm from the upwind end of the working section. Airflow direction is away from the reader

As the MWT is a duct with a fully developed flow the shear stress and the friction velocity are calculated by measuring the pressure gradient not by the traditional approach of using logarithmic velocity profiles [5, 15, 19, 20]. Pressure drop along the length of a duct is well understood within fluid mechanics [21, 22]. The approach taken here is to partition the contribution that an open floor (one wall of the duct) has on the total duct pressure gradients in order to calculate the shear stress and the friction velocity on that surface. The following describes the approach taken.

Internal flow within a duct is constrained by bounding walls and the viscous effect which permeates the entire flow. Inviscid flow enters the duct and viscous boundary layers flow downstream retarding the axial flow *u(y,z)* at the wall, thereby accelerating the centre of the flow to maintain the incompressible continuity requirement [21].

$$Q = \int_A u(y,z)\, dA = constant \tag{1}$$

Where Q is volume flow, u(y,z) is flow velocity and A is cross sectional area. At a finite distance from the entrance the boundary layers merge and the inviscid core disappears. The duct flow then is entirely viscous and the axial velocity adjusts until it is fully developed. The distance (*x*) downstream that this occurs is referred to as the entrance length (L_e). Downstream of $x \geq L_e$ the velocity profile u(y,z) is constant, wall shear is constant and pressure drops linearly with *x* for either laminar or turbulent flow. Dimensional analysis indicates the Reynolds number (R_e) is the only parameter affecting entrance length L_e. Re_m is the Reynolds number for the MWT and calculated by

$$Re_m = \frac{\rho U}{v} D_h \tag{2}$$

$$= \omega D_h \tag{3}$$

where U is the average flow velocity, ρ is the density of air, v is the viscosity of air, D_h is the hydraulic diameter, and ω is the scaled flow velocity. In a rectangular duct, the hydraulic diameter is determined as

$$D_h = \frac{2\ x\ area}{width + height} \tag{4}$$

The MWT has Reynolds numbers ranging from 26,500 < Re_m < 80,000 (i.e. fully turbulent flow) [22]. In ducts with turbulent flows, the boundary layers grow faster and L_e is relatively short:

$$\frac{L_e}{D_h} \approx 4.4 Re_m^{\frac{1}{6}} \tag{5}$$

Therefore whilst the MWT does not support a log profile, the entrance length (*L_e*) effect is restricted within the transition section of the tunnel leaving the fully developed flow region to occur within the working section (Figure 1). This is important because it is in the working section that a developed velocity profile $u(y, z)$ needs to occur if changes in surface roughness are to be determined.

In larger wind tunnels the surface roughness is calculated from the wind profile. However, the micro wind tunnel does not support a log profile, thus an alternative technique for calculating u_*, the friction velocity, is required. The friction velocity (u_*) is frequently used to measure the wind speed required to initiate sediment movement.

The integral momentum method [23 in 24] is used here to calculate u_*. This paper shows that the friction velocity can be determined by measuring pressure gradients and using integral momentum balance. Theoretically, in a fully developed duct flow, the integral momentum balance is:

$$\int_p \rho u_*^2 \, dP = -A \frac{dp}{dx} \tag{6}$$

where u_* is the friction velocity, ρ is air density, ρu_*^2 is the drag on the surface of the duct, *P* is the perimeter of the duct, *dP* is increment of the perimeter, *A* is the cross-sectional area of the duct and $\frac{dp}{dx}$ is the stream-wise pressure gradient. Therefore, in a rectangular duct of height *Z* and breadth *Y*:

$$2(Y+Z)u_{*a}^2 = -\frac{YZ}{\rho}\frac{dp}{dx} \tag{7}$$

where $u_{*\alpha}$ is an area-weighted average friction velocity for all surfaces around the tunnel circumference. The turbulence and secondary flow within the duct as documented by Schetz and Allen [22] act to equalise the shear stress across the perimeter of the duct. Thus, it is possible to partition the friction velocity to the various surfaces, hence the floor contributes a length *Y* to this average and the sides and roof together contribute a length (2*Z* + *Y*). Consequently:

$$2(Y+Z)u_{*a}^2 = Yu_{*f}^2 + (2Z+Y)u_{*s}^2 \tag{8}$$

where u_{*f} is the friction velocity for the rough floor and u_{*s} is the friction velocity for the smooth sides and roof. Equating Equations 7 and 8 gives:

$$Yu_{*f}^2 + (2Z+Y)u_{*s}^2 = -\frac{YZ}{\rho}\frac{dp}{dx} \tag{9}$$

Determining the friction velocity for the rough floor (u_{*_f}) can therefore be inferred from measurements of the pressure gradient ($\frac{dp}{dx}$) by re-arranging Equation 8 as:

$$u_{*f}^2 = -\left(\frac{2Z}{Y} + 1\right) u_{*s}^2 - \frac{Z}{\rho}\frac{dp}{dx} \quad (10)$$

Now u_{*_s} can be determined by noting that when u_{*_f} = u_{*_s}, Equation 8 becomes:

$$2(Z + Y)u_{*a}^2 = (2Z + 2Y)u_{*s}^2 \quad (11)$$

Equating Equations 7 and 11 gives:

$$u_{*s}^2 = -\frac{YZ}{2(Z+Y)\rho}\frac{dp}{dx}|_s \quad (12)$$

Where $\frac{dp}{dx}|_s$ denotes the pressure gradient when all four surfaces are smooth. Hence, u_{*_f} can be related to current pressure gradient ($\frac{dp}{dx}$) and the smooth pressure gradient ($\frac{dp}{dx}|_s$) by:

$$u_{*f}^2 = -\frac{Z}{\rho}\left[\frac{dp}{dx} - \frac{(2Z+Y)}{2(Z+Y)}\frac{dp}{dx}|_s\right] \quad (13)$$

Finally, the surface roughness (Z_0) can be estimated from the central flow characteristics of the duct:

$$z_0 \approx \frac{25 \ x \ 10^{-3}}{\exp\left(\frac{ku_c}{u_{*f}}\right)} \quad (14)$$

where u_c is the measured velocity in the centre of the duct (z = 25 mm) and k = von Karman's constant (0.4).

These theoretical workings were tested by measuring the pressure gradient for the transition and working sections of the tunnel over three test surfaces (under both transition and working sections). These three surfaces are; smooth (4 mm ABS plastic, 'glassy' side up), medium (213 micron sand spray-glued to PVC) and rough (bubble-wrap with bubble 10 mm diameter, 5 mm high). Results in Table 1 show that as the test surface roughness increased, so did u_{*f}, indicating that the pressure gradient method is sensitive to scaling issues within the MWT. This increases confidence that drag coefficient can be partitioned.

Table 1 Flow descriptors for the MWT calculated using the pressure gradient method (Raupach et al. 2006) for the flow on the tunnel floor. Wind speeds measured using the roof mounted pressure ports (pressure port measurements at x = 200 and 900, y = 50, z = 50).

Tunnel speed m s^{-1}	Test surface	Coefficient of drag (unitless)	u_* (m s^{-1})	z_o (mm)
6.8	Smooth	0.0023	0.32	0.006
6.8	Medium	0.0034	0.40	0.026
6.8	rough	0.0059	0.52	0.139
11.6	Smooth	0.0021	0.54	0.004
11.6	Medium	0.0034	0.68	0.027
11.6	rough	0.0056	0.86	0.117

The data in Table 1 compare well with u_* values of 0.35 m s^{-1} (U=6.8 m s^{-1}) and 0.72 m s^{-1} (U=11.6 m s^{-1}) obtained by Shao and Raupach [25] who tested on a bed of 200 µm sand using a large portable wind tunnel. This result suggests that the MWT produces comparable surface drag for the wind speeds in the tunnel. Figure 4 shows the relationship between tunnel velocity and friction velocity for the MWT.

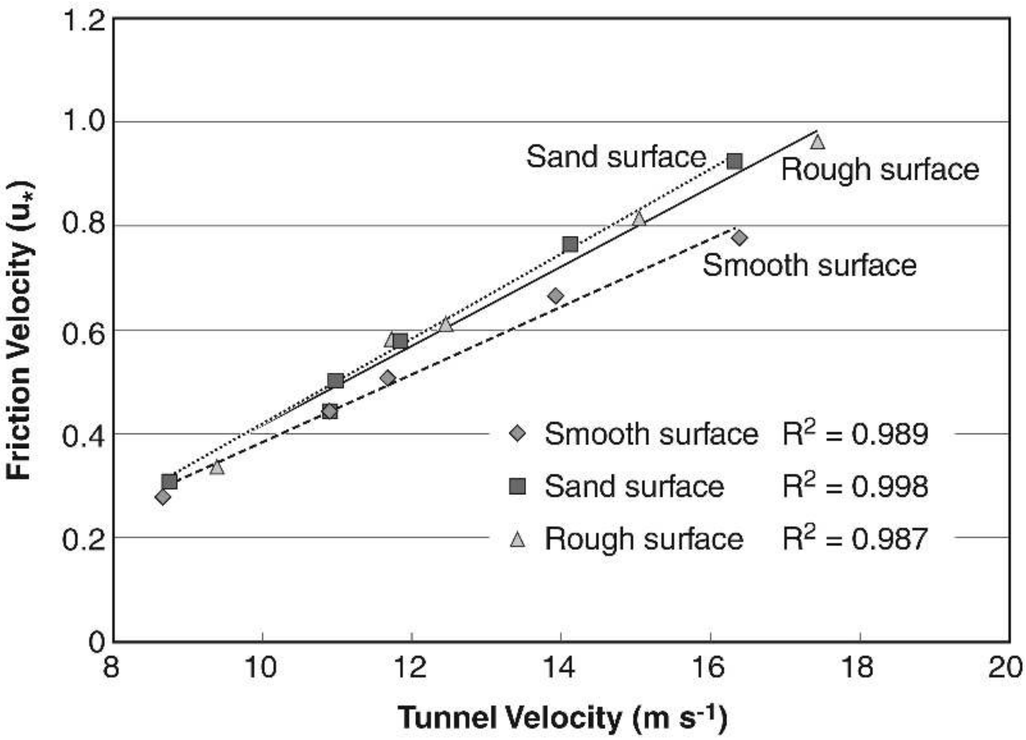

Fig. 4 Relationships between the tunnel velocity and u_* for each of the three tested surfaces (smooth (z < 0.01 mm), medium (z ~ 0.1 mm) and rough (z ~ 2 mm)). Wind speeds measured using the roof mounted pressure ports (pressure port measurements at x = 200 and 900, y = 50, z = 50). All standard errors lie within +/- 0.002 of the mean values

2.3 Saltation injection, collection efficiency and operation procedures

Saltation injection is used in a wind tunnel to achieve saturated saltation flow. In the field saturated saltation will develop over much longer distances than can be reproduced in the working sections of portable wind tunnels [20, 25]. Saltation sands should therefore be delivered at a flux rate sufficient to produce saltation rates observed in the field, and have known physical properties (size, chemical composition).

Commercially available sand with a unimodal size of 213 microns and 99 % quartz content is used in the MWT saltation injection system. Without the tunnel operating (tunnel velocity = 0 ms^{-1}) the saltation flux rate is 6.1±0.1 g $m^{-1}s^{-1}$. As the tunnel airflow velocity increases (tunnel velocity = 5–16.1 ms^{-1}) so too does the saltation flux rate, ranging from 7.5-10.8 g $m^{-1}s^{-1}$ (Figure 5). Saltation flux rates are slightly higher than those reported by Pietersma et al. [26] who had an adjustable saltation feed rate of 0.25-6.6 g $m^{-1}s^{-1}$, but lower than Van Pelt et al., [5] who had an adjustable saltation feed rate of 10-30 g $m^{-1}s^{-1}$. The range of saltation flux rates for the MWT is within the variability reported for other wind tunnels and therefore differences considered inconsequential.

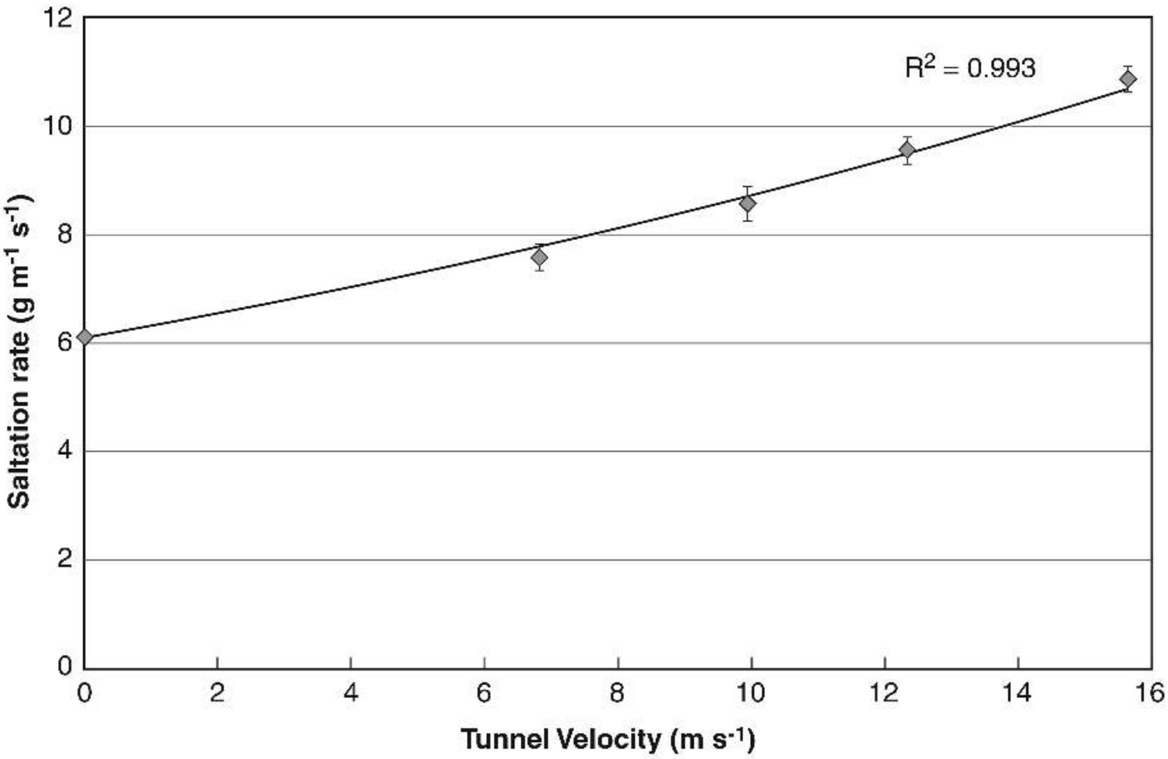

Fig. 5 Saltation flux rate is 6.1 g $m^{-1}s^{-1}$ with no tunnel flow but increases (7.5-10.8 g $m^{-1}s^{-1}$) as tunnel velocity increases. Each velocity was replicated five times measured using pitot-static tubes at x = 900, y = 50, z = 25 and all standard errors lie within +/- 0.07 of the mean values

The collection efficiency of the sediment sampler was tested by adding a known amount of saltation sand. The sampler inlet has a cross-section of 10 x 50 mm representing 10 % of the cross-sectional area of the tunnel. For four wind speeds (each repeated five times) 30 g of saltation sand was added via the saltation injection system at the start of the one minute run (using a smooth test bed). Assuming that the sediment sampler is 100 % efficient, 3 g of sediment should be collected at the end of each run. The ratio of collected sediment to that expected shows that on the smooth test surface, the sampling efficiency was greater than 95 % for wind speeds higher than 10 ms^{-1} but dropped to 85 % at lower wind speeds (Figure 6). A change in trapping efficiency with wind speed is commonly observed in semi-isokinetic samplers [27]. On rough surfaces the expectation is that sediment will be trapped by roughness elements reducing the amount of sediment reaching the sampler. Understanding the trap efficiency means that the storage potential of different surfaces can be estimated [24].

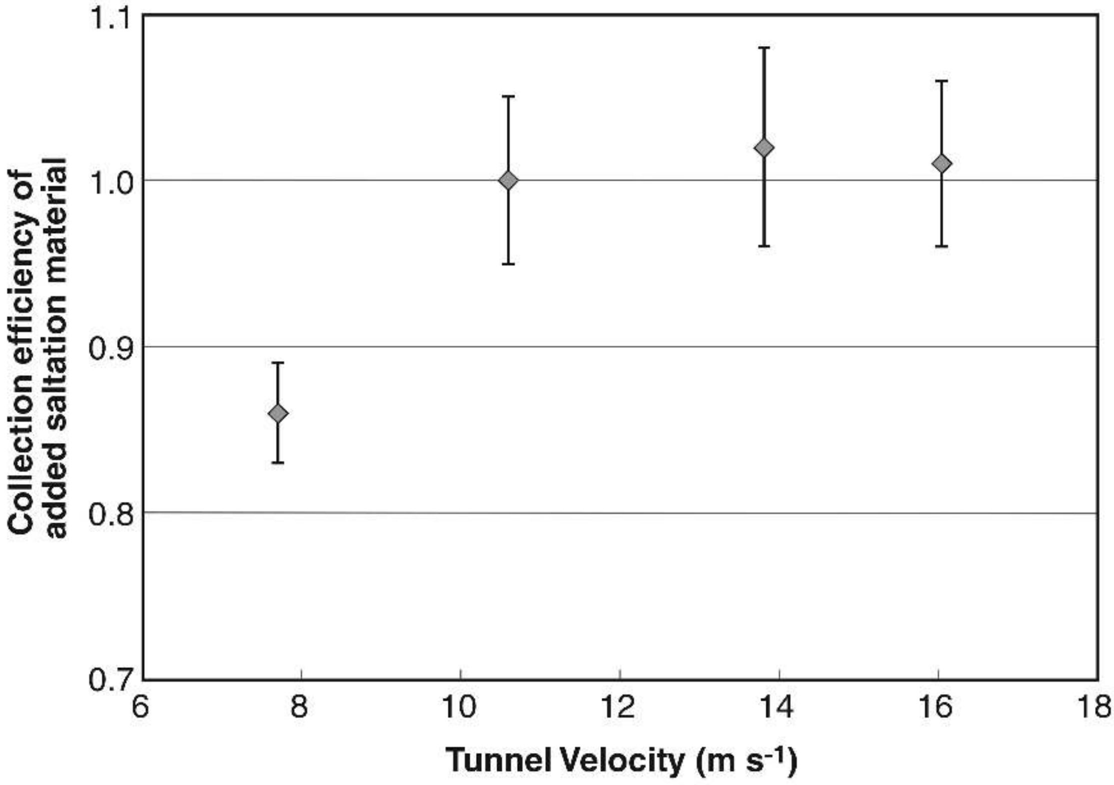

Fig. 6 Collection efficiency of the sediment sampler indicates that over a smooth test surface the tunnel is very efficient at collecting the expected 10 % sediment flow released in the tunnel at wind speeds greater than 10 m s^{-1}. The tunnel under samples at tunnel velocities less than 8 m s^{-1} (baffle position 2). Each velocity was replicated five times measured using pitot-static tubes within the tunnel flow at x = 900, y = 50, z = 25 and sediment trap line. All standard errors lie within +/- 0.05 of the mean values

Operating the MWT uses two approaches to saltation impact. The first approach relies on any naturally-available, loose, erodible material to act as a saltation source. Wind-removed sediment is collected on 125 mm-diameter glass-fibre filter paper with 0.1 µm pores, and weighed. Sediment flux (Q) (g $m^{-1}s^{-1}$) with no added saltation material is calculated as:

$$Q = \frac{mass}{[0.01m^2 \times 60s]} \quad (10)$$

The second approach uses the addition of saltation material as described above to initiate the breakdown and removal of fine sediments through abrasion process. Saltation induced sediment flux (Q_{SI}) (g $m^{-1}s^{-1}$) is calculated as:

$$Q_{SI} = \frac{[mass - 3g]}{[0.01m^2 \times 60s]} \quad (11)$$

where mass is the weight (g) of sediment collected on the filter paper and $0.01m^2$ is the footprint of the MWT working area. This equation assumes that all the sediment introduced at the upwind end reaches the sediment sampler at the downwind end. This is a reasonable assumption for a smooth surface with no storage capacity. As highlighted above rough surfaces can trap sediments and there is potential to use the MWT to increase the understanding of this however it will not be explored further in this paper. To identify the susceptibility of a surface to abrasion, the ratio of Q_{si} : Q is used to describe the saltation entrainment ratio, quantifying how much more sediment was lost with the addition of saltation sand. The higher the number the greater impact of the saltation sands.

The use of a range of wind speeds on all surfaces provides an indication of how sediment flux changes with wind speed. Comparison between the surfaces requires a standard wind speed to act as a default comparison. The chosen wind speed was u = 9 m s^{-1} as this typically causes sediment entrainment in the field [28, 29].

2.4 Summary of development and calibration

The MWT has been shown to produce velocities ranging from 5 to 18 m s^{-1} with high reproducibility. Wind velocities are laterally uniform (+/- 0.2 m s^{-1}) and values of u_* at the tunnel bed (calculated using the integral momentum method) are comparable with those from larger tunnels where logarithmic, profiles can be developed [25,5]. To account for the variability in the saltation feed rate as velocity increases, known amounts of saltation sediment were used for all runs. A high collection efficiency (>85 %) was reported across a range of tunnel velocities. The MWT therefore achieves the three fundamental wind tunnel design critieria proposed by Maurer et al., [13] of, producing wind speeds and aerodynamic flows that reflect natural conditions, along with being easy to transport, assemble and operate.

3 Research Applications of the MWT

The second half of this paper provides three contrasting examples of where the MWT has been used in field research in order to illustrate the practicality of its use.

3.1 Wind erosion of rangeland soils

A field study was undertaken in semi-arid rangelands near Longreach, Queensland, Australia to assess the impact of different stocking pressures from cattle and sheep grazing on soil erodibility to wind [30]. Wind erosion simulations were conducted along a grazing gradient (from high to low) leading away from a stock watering point; following the design of Pickup [31]. Field experiments were conducted on two soil types, a cracking clay soil (23°36’44.8”S; 143°17’46.9”E) and a sandy loam (30°27’14.7”S; 141°44’32.4”E).

Both sites were vegetated with annual and perennial grasses. As the focus of the study was upon soil erodibility (rather than the protection to soils afforded by vegetation) it was important to exclude grasses from the wind tunnel simulation sites. The MWT was highly suitable to this application because its small footprint could fit between the grass clumps (Fig. 7). This project would not have been feasible with a conventional field wind tunnel, because grasses could not have been excluded from the large working section of such a tunnel.

Fig. 7 The micro wind tunnel was highly suitable to deployment in a grassed rangeland site because its small footprint could fit between grass clumps

Sediment flux was measured along the grazing gradient using the MWT, but only two points along this transect are reported here. The highest stocking rate and soil surface disturbance zone was closest to the watering point and a low stocking rate and disturbance zone was 2000 m from the watering point.

Table 2 Measured sediment flux (g/m^2/s) at two disturbance zones on two soil types using one MWT wind speed, U = 9 m s^{-1}. Q is sediment flux with only wind blowing across soil surface. Q_{SI} is the sediment flux with saltation sediment added to the tunnel runs

	Sediment flux (g/m^2/s)			
	Clay site		Sandy loam site	
	High disturbance zone	Low disturbance zone	High disturbance zone	Low disturbance zone
Without saltation added (Q)	3.35	0.04	9.59	2.64
With saltation added (Q_{SI})	5.66	0.31	13.47	3.39
Saltation entrainment ratio (Q_{SI} : Q)	x 1.7	x 7.8	x 1.4	x 1.3

Three results of the MWT simulations are shown in Table 2.

1. Overall wind erosion rates, measured as sediment fluxes (Q), are higher on sandy loam soils than clay soils; confirming the widely reported result that increasing the sand content of soils increases their erodibility [32].

2. Disturbance of soil surfaces increases sediment fluxes on both soils but the relative impact is much greater on the clay soil than on the sandy loam soils. This suggests that clay soils are more vulnerable to increased stocking rates than sandy soils.

3. If saltation sands are present in the windflow sediment fluxes are increased to a much greater extent on clay soils (x 1.7 to x 7.8) than sandy loam soils (x 1.3 to x 1.4); confirming the earlier result that the presence of sands increases soil erodibility.

This study provides new and useful understanding of changes in soil erodiblity in response to variations of grazing pressure. The results suggest that spatial variations of soil surface disturbance induced by grazing pressure have a direct impact on soil erodibility to wind. The MWT played a crucial role in this project because its small footprint enabled the positioning of the tunnel between grass clumps; thus testing the soil surface conditions avoiding the complicating effects of vegetation upon wind erosion.

3.2 Wind erosion on alluvial claypans

A field study was undertaken on a claypan on the Diamantina River floodplain, Queensland. Claypans as a single unit (covering from 1 – 100s square kilometres in size) are known to be dust source hotspots [32, 33]. However claypans do not comprise uniform surfaces and instead are characterised by a complex mosaic of surface crust types. The aim of this study was to determine the relative erodibility of each crust type. The erodibility of individual crust types is poorly understood in part because most large portable wind tunnels cover a range of crust types in a single run, thereby homogenising the results. Field experiments were conducted on three crust types; structural, depositional and biological as defined by Valentin and Bresson [34] and Thomas and Dougill [35]. The MWT was used both without and with saltation added.

Across the claypan, the sediment flux varied considerably (at u = 9 m s^{-1}), with biological crust surfaces yielding a higher sediment flux (Q) than the depositional and structural crusts (Table 3). Sediment flux with saltation added (Q_{SI}) is again higher from the biological crusts than the structural and depositional (Table 3). At first sight, these results appear to be inconsistent with other published studies [16,17] which conclude that biological crusts provide greater protection to soils than physically crusted or depositional surfaces. In reality the results probably reflect the capacity of biological crusts to store loose sediment and release it when wind speeds increase. The proportional increase in sediment flux with the addition of saltation sands (Q_{SI} : Q) is much less for biological crusts (x 5.6) than depositional and structural crusts (x14 and x 16 respectively), indicating that biological crusts are more protective of soils in a saltation impact environment. This result reinforces the earlier interpretation; that the relatively high overall sediment fluxes from biological crusted surfaces reflect their capacity to store loose sediment and release it when wind speeds increase.

This result also supports the conclusions from the study by Hupy [36] which showed that the spatial positioning of different surface types can have an important influence upon overall wind erosion rates from a claypan. Hupy [36] found that storage zones of saltation sands, such as the biological crusted regions, provided a source of abrasion material for downwind sites.

Table 3 Measured sediment flux (g/m^2/s) at three surface crust types using one MWT wind speed, U = 9 m s^{-1}

	Sediment flux (g/m^2/s)		
	Structural crust	Depositional crust	Biological crust
Without saltation added (Q)	0.109	0.316	1.117
With saltation added (Q_{SI})	1.766	4.371	6.196
Saltation entrainment ratio (Q_{SI} : Q)	x 16	x 14	x 5.6

This study provides new and useful understanding of the changes in soil erodiblity across a heterogenous claypan surface. The results suggest that spatial variations of crust types have a direct impact on erodibility and that both the abundance and spatial distribution of the crust types have an effect of the overall sediment flux of a claypan as a whole. The use of the MWT was crucial to the collection of this sediment flux data as its small nature and portability enabled the testing of discrete crust types. Larger field tunnels would have measured the response of either a range of crust types, and/or the patchy vegetation which is commonly associated with the biological crusts on claypans.

3.3 Erodibility of iron ore sediments

A field study was undertaken to assess the relative erodibility of different iron ore sediments within an iron ore port facility in Western Australia. The iron ore storage facility involved receiving, sorting, stacking, transporting via conveyors and ship loading several different ore products. This diverse range of products and material handling activities produced considerable fugitive dust which can have negative impacts upon local communities. The term fugitive dust refers to dust which is mechanically entrained [37] and may be wind-eroded at mine sites, ore storage areas and mine rehabilitation areas [38, 39]. One measure of the fugitive dust potential of an ore deposit is the surface sediment fluxes resulting from increased wind speeds. Identifying the key sources of dust is an important precursor to applying appropriate dust mitigation strategies. The MWT was used to measure the wind erodibility of different iron ore deposits. MWT measurements were carried out on two iron ore stockpiles and two local ore deposits; on roadsides and beneath the conveyor belts (Table 4).

Table 4. Measured sediment flux ($g/m^2/s$) at two iron ore sites and two deposited sediment sites using one MWT wind speed, $U = 9\ m\ s^{-1}$

	Sediment flux ($g/m^2/s$)			
	Iron Ore surfaces		Deposited sediments	
	Stockpile 1	Stockpile 2	Deposits on road	Deposits below conveyor
Without saltation added (Q)	1.41	0.01	78.13	4.35
With saltation added (Q_{SI})	2.65	0.49	159.08	32.93
Saltation entrainment ratio (Q_{SI} : Q)	x 1.9	x 49.0	x 2.0	x 7.5

The highest overall sediment fluxes were recorded on the local ore deposits (on road and under conveyor) and the lowest from the two stockpile ores (Table 4). The very high fluxes on the local ore deposits arose because they were relatively fine dust deposits (< 50 μm), with low compaction. These deposits were therefore a major potential source of fugitive dusts. The sediment fluxes with saltation material in the airflow (Q_{SI}) were increased on all sites. While the proportional increase in sediment flux (Q_{SI} : Q) was greatest on the stockpile 2, the absolute sediment flux was much lower than on the local deposits. The large range in sediment fluxes between sites highlights the complexity of managing fugitive dust emissions at mine sites and iron ore storage areas and the need to adopt a range of different dust mitigation strategies.

The MWT proved to be very well suited to the practical demands of operating at this industrial site; where equipment access and operation was difficult, especially on inclined stockpile surfaces and beneath conveyor belts.

3.4 Summary of applications of the micro wind tunnel

The MWT has proved to be a valuable tool for assessing small scale soil erodibility issues. The use of the MWT across a range of surfaces provides new and useful understanding of the erodibility of rangelands, claypans and ore stockpiles. There are 3 key attributes of the MWT. First, nimbleness, second flexibility, third operability. The MWT "nimbleness" in getting in and around grass clumps which are a common feature of many rangelands and difficult to measure with larger tunnels provides a true practical advantage. The tunnel is "flexible" in being easily deployed across diverse terrains and in constricted industrial settings. Truck or trailer mounted portable wind tunnels are well suited to large open agricultural paddocks, therefore to apply these tools in a spatially restricted environment often means the test surfaces have to be disturbed and brought to the tunnel, thus altering their natural erodibility properties. Another important feature of the MWT is its "operability". This tunnel can be used, packed up and transported by one person. Larger portable tunnels require multiple people and often heavy lifting aids to assemble and pack the equipment.

4 Conclusion

The micro wind tunnel (MWT) is a small, portable wind tunnel, operable by one person. The MWT produces airflow velocities ranging from 5 to 18 m s^{-1} with high reproducibility. The velocity profiles show an orderly progression downwind, and the across tunnel contour plots showed a good air speed distribution. Unlike larger wind tunnels, the dimensions of the MWT limit the form of velocity distribution in the working section, but it is these duct like dimensions that enable the shear stress within to be determined from the pressure drop. Through measuring the pressure gradients enables the measurement of drag coefficient and allows the calculation of both sensible u_* and surface-roughness measures in the MWT. Saltation feed into the airflow is at the optimal rate of 6.1 g $m^{-1}s^{-1}$ and collection efficiency is high.

The utility of the MWT is demonstrated from wind erosion studies on rangelands and alluvial claypans, and at an iron ore storage facility. The rangeland study highlights the ease of use of the MWT on surfaces with complex patterns of tufted pasture grasses. At the claypan site the small footprint of the MWT allowed wind erosion simulations to be conducted on different discrete surface crust types. At the iron ore storage facility the MWT proved to be very well suited to the practical demands of operating at an industrial site; where equipment access and operation were difficult; on inclined stockpile surfaces and beneath conveyor belts. The MWT is therefore a valuable wind erosion simulation tool which very well supplements larger portable field wind tunnels.

Acknowledgements

The authors acknowledge the major contribution to the design and construction of the MWT by their late co-author Mike Raupach who passed away recently. Mike's passing is a great loss to our research community. Thanks to Samantha McMillan for initial testing and development work on the MWT. This work was partially funded by the UK NERC (NE/K011461/1) and Griffith University.

Reference

1. Leys JF (1999) Wind Erosion on Agricultural Land. *In* 'Aeolian Environments, Sediments and Landforms'. (Eds. Gouldie, A. S., Livingstone, I., and Stokes, S.), pp. 143-166 (John Wiley and Sons).

2. Webb NP, Strong CL (2011) Soil erodibility dynamics and its representation for wind erosion and dust emission models. Aeolian Research 3:165-179

3. Zobeck TM (1991) Abrasion of crusted soils: Influence of abrader flux and soil properties. SSSAJ. 55(4): 1091-1097

4. Goossens D, and Offer ZY (2000) Wind tunnel and field calibration of six Aeolian dust samplers. Atmospheric Environment. 34(7): 1043-1057

5. Van Pelt RS, Zobeck TM, Baddock MC, Cox JJ (2010) Design, construction and calibration of a portable boundary layer wind tunnel for field use. Transactions of the American Society of Agricultural and Biological Engineers 53(5):1-10

6. Etyemezian V, Nikolich G, Ahonen S, Pitchford M, Sweeney M, Gillies J and Kuhns H (2007) The Portable In-Situ Wind Erosion Laboratory (PI-SWERL): A new method to measure windblown dust properties and potential for emissions Atmos Environ 41:3789–3796

7. Hagen LJ (2004) Evaluation of the Wind Erosion Prediction System (WEPS) erosion submodel on cropland fields. Environmental Modelling and Software 19: 171–176

8. Webb NP, McGowan HA, (2009) Approaches to modelling land erodibility by wind. Progress in Physical Geography 33:587–613

9. Butler HJ, Hogarth WL, and McTainsh GH (1996) A source-based model for describing dust concentrations during wind erosion events: an initial study. Environmental Software 11(1-3):45-52

10. Bagnold RA (1941) The physics of blown sand and desert dunes. William Morrow & Company, New York

11. Chepil WS (1953) Field structure of cultivated soils with special reference to erodibility by wind. Soil Science Society Proceedings 185-190

12. Zhang YM, Wang HL, Wang XQ, Yang WK and Zhang DY (2006) The microstructure of microbiotic crust and its influence on wind erosion for a sandy soil surface in the Gurbantunggut Desert of Northwestern China. Geoderma 132:441–449

13. Maurer T, Hermann L, Gaiser T, Mounkaila M, Stahr K (2006) A mobile wind tunnel for wind erosion field measurements. Journal of Arid Environments 66(2):257-271

14. Nickling WG and Gillies JA (1993) Dust emission and transport in the Male, West Africa. Sedimentology 40:859-868

15. Gillette DA (1978) Tests with a portable wind tunnel for determining wind erosion threshold velocities. Atmospheric Environment 12:2309-2313

16. Belnap J and Gillette DA (1997) Disturbance of biological soil crusts: impacts on potential wind erodibility of sandy desert soils in southeastern Utah. Land Degradation and Development 8:355-362

17. Belnap, J. and Gillette, DA (1998) Vulnerability of desert biological soil crusts to wind erosion: the influences of crust development, soil texture, and disturbance. Journal of Arid Environments 39:133-142

18. Sweeney M, Etyemezian V, Macpherson T, Nickling W, Gillies J, Nikolich G, McDonald E (2008) Comparison of PI-SWERL with dust emission measurements from a straight-line field wind tunnel. Journal of Geophysical Research 113:(F01012) doi:10.1029/2007/JF000830

19. Zingg AW (1951) A portable wind tunnel and dust collector development to evaluate the erodibility of field surfaces. Agronomy Journal 43(2):189-191

20. Raupach MR and Leys JF (1990) Aerodynamics of a portable wind erosion tunnel for measuring soil erodibility by wind. Australian Journal of Soil Research 28(2):177-191

21. White FM (1994) Fluid Mechanics. McGraw-Hill, New York

22. Schetz JA and Fuhs AE (1999) Fundamentals of fluid mechanics. John Wiley and Sons, New York

23. Batchelor GK (1967) An Introduction to Fluid Dynamics. Cambridge University Press, Cambridge

24. Raupach MR, Hughes DE and Cleugh HA (2006) Momentum absorption in rough-wall boundary layers with sparse roughness elements in random and clustered distributions. Boundary-Layer Meteorology 120:201-218

25. Shao Y and Raupach MR (1992) The overshoot and equilibration of saltation. Journal of Geophysical Research 97(20):559-564

26. Pietersma D, Stetler LD and Saxton KE (1996) Design and aerodynamics of a portable wind tunnel for soil erosion and fugitive dust research. Trans of the ASAE 39:2075-2083

27. Goossens D and Offer ZY (2000) Wind Tunnel and field calibration of six Aeolian dust samplers. Atmospheric Environment 12(12):1043-1057

28. McTainsh GH, Leys JF, and Nickling WG (1999) Wind erodibility of arid lands in the channel country of Western Queensland, Australia. Zeitschrift fur geomorphologie 116:113-130

29. Gillette DA, Adams J, Muhs D and Kihl R (1982) Threshold friction velocities and rupture moduli for crusted desert soils for the imput of soil particles into the air. Journal of Geophysical Research 87:9003-15

30. Aubault HA (2014) Estimating the impacts of pastoral activities upon wind erosion in the arid and semi-arid rangelands of eastern Australia. Ph.D. Thesis, Griffith University

31. Pickup G (1989) New land degradation survey techniques for arid Australia: problems and prospects. Aust. Rangel. J. 11:74-82.

32. McTainsh GH and Leys JF (1993) “Chapter 7 - Wind erosion”. In: McTainsh GH and Boughton WC (Eds) Land degradation processes in Australia. Longman-Cheshire, Melbourne pp188-233

33. Reheis MC (2006) A 16-year record of eolian dust in Southern Nevada and California, USA: controls on dust generation and accumulation. Journal of Arid Environments 67:487-520

34. Valentin C and Bresson LM (1992) Morphology, genesis and classification of surface crusts in loamy and sandy soils. Geoderma 55:225-245.

35. Thomas AD and Dougill AJ (2006) Distribution and characteristics of cyanobacterial soil crusts in the Molopo Basin, South Africa. Journal of Arid Environments 64:270-283

36. Hupy JP (2004) Influence of vegetation cover and crust type on wind-blown sediment in a semi-arid climate. Journal of Arid Environments 58:167-179

37. Gillies JA, Watson JG, Rogers CF, Dubois D, Chow JC, Langston R, and Sweet J (1999) Long-Term Efficiencies of Dust Suppressants to Reduce PM 10 Emissions from Unpaved Roads. Journal of the Air & Waste Management Association 49:3–16

38. Cowherd C Jr, Bohn R and Cuscino T (1979) Iron and steel plant open source fugitive emission evaluation; Report No EPA-600/2-79-103. Research Triangle Park, NC, U.S. Environmental Protection Agency, Industrial Environmental Research Laboratory

39. Chan Kon L, Durucan S and Korre A (2007) The development and application of a wind erosion model for the assessment of fugitive dust emissions from mine tailings dumps. International Journal of Mining, Reclamation and Environment 21(3):198-218